Lattice Boltzmann model with self-tuning equation of state for multiphase flows

Rongzong Huang,[1,2,*] Huiying Wu,[1,†] and Nikolaus A. Adams[2,‡]

[1]*School of Mechanical Engineering, Shanghai Jiao Tong University, 200240 Shanghai, China*
[2]*Institute of Aerodynamics and Fluid Mechanics, Technical University of Munich, 85748 Garching, Germany*

A lattice Boltzmann (LB) model for multiphase flows is developed that complies with the thermodynamic foundations of kinetic theory. By directly devising the collision term for the LB equation at the discrete level, a self-tuning equation of state is achieved, which can be interpreted as the incorporation of short-range molecular interaction. A pairwise interaction force is introduced to mimic the long-range molecular interaction, which is responsible for interfacial dynamics. The derived pressure tensor is naturally consistent with thermodynamic theory, and surface tension and interface thickness can be independently prescribed. Numerical tests, including static and dynamic cases, are carried out to validate the present model and good results are obtained. As a further application, head-on collision of equal-sized droplets is simulated and the elusive "bouncing" regime is successfully reproduced.

I. INTRODUCTION

The lattice Boltzmann (LB) method, first introduced in 1988 [1], uses a set of distribution functions with discrete velocities to depict complex fluid flows. Due to its kinetic nature, the LB method shows potential for considering microscopic and mesoscopic interactions. It is therefore believed that this method is particularly suitable for multiphase flows, which are complex at the macroscopic level but are much simpler from the microscopic viewpoint. The applications of the LB method to multiphase flows emerged in the early 1990s [2] and have significantly increased in the past decade [3].

Although various LB models for multiphase flows exist [4–6], criticisms have been raised for a long time [7,8]. In the pseudopotential LB model [4,9], a pairwise interaction force is used to mimic the microscopic interaction, which can recover nonideal-gas effects and interfacial dynamics at the same time. However, such simultaneous recoveries make this model suffer from thermodynamic inconsistency, though significant progress has been made in approximating the coexistence densities close to the thermodynamic results [10–12]. In the free-energy LB model [5,13], the thermodynamically consistent pressure tensor is directly incorporated to produce the dynamics of multiphase flows. Thus, the annoying evaluations of (high-order) derivatives are unavoidable, though improvements have been made to remedy the violation of Galilean invariance in this model [14–17]. Different from the pseudopotential and free-energy models, the multiphase LB model has also been developed from kinetic theory via systematic discretization procedures [6,8]. Complicated equivalent force terms exist in this model and severe numerical instability is encountered. Improved models were formulated

[18,19] at the price of sacrificing the underlying physics and computational simplicity.

In this work, we develop an LB model for multiphase flows complying with the thermodynamic foundations of kinetic theory analyzed by He and Doolen [8]. The underlying molecular interaction responsible for multiphase flows is divided into short-range and long-range parts, which are incorporated by constructing an LB model with self-tuning equation of state (EOS) and introducing a pairwise interaction force, respectively. The present LB model has the advantages of the popular pseudopotential and free-energy LB models and is free of the aforementioned drawbacks. The remainder of this paper is organized as follows. In Sec. II, an LB model with self-tuning EOS is developed, and in Sec. III, the application of this model to multiphase flows is analyzed and discussed. Numerical tests are then carried out in Sec. IV to validate the present LB model for multiphase flows, and a brief conclusion is drawn in Sec. V.

II. LB MODEL WITH SELF-TUNING EOS

With the presence of a discrete force term $F_{v,i}$, the LB equation for the density distribution function f_i can be generally expressed as [20,21]

$$
\begin{aligned}
f_i(\mathbf{x} &+ \mathbf{e}_i \delta_t, t + \delta_t) \\
&= f_i + \delta_t F_{v,i} - \Lambda_{ik}\left(f_k - f_k^{\text{eq}} + \frac{\delta_t}{2} F_{v,k}\right) \\
&\quad - \Gamma_{ij}\left(\delta_{jk} - \frac{\Lambda_{jk}}{2}\right)\left(f_k - f_k^{\text{eq}} + \frac{\delta_t}{2} F_{v,k}\right) \\
&\quad - \delta_x \mathbf{\Theta}_i \cdot \nabla \rho - \frac{\delta_x}{c^2} \mathbf{\Phi}_i \cdot \nabla p_{\text{LBE}},
\end{aligned}
\tag{1}
$$

where $\mathbf{e}_i$ is the discrete velocity, Λ_{ik} is the collision matrix in discrete velocity space, and the right-hand side (RHS), termed the collision process, is computed at position $\mathbf{x}$ and time t. On the RHS of Eq. (1), the last three correction terms are introduced to eliminate the additional cubic terms of velocity

*rongzong.huang@tum.de
†whysrj@sjtu.edu.cn
‡nikolaus.adams@tum.de

in the recovered macroscopic equation at the Navier-Stokes level [20], where p_{LBE} denotes the EOS directly recovered by the LB equation. Owing to the explicit physical significance of the moments of distribution function, it is more convenient to construct the collision term in moment space than in discrete velocity space. Orthogonal moments without weights are adopted [22], and the RHS of Eq. (1) is transformed into moment space:

$$\bar{\mathbf{m}} = \mathbf{m} + \delta_t \mathbf{F}_m - \mathbf{S}\left(\mathbf{m} - \mathbf{m}^{\text{eq}} + \frac{\delta_t}{2}\mathbf{F}_m\right) - \mathbf{R}\left(\mathbf{I} - \frac{\mathbf{S}}{2}\right)\left(\mathbf{m} - \mathbf{m}^{\text{eq}} + \frac{\delta_t}{2}\mathbf{F}_m\right) - \delta_x \mathbf{T} \cdot \nabla\rho - \frac{\delta_x}{c^2}\mathbf{X} \cdot \nabla p_{\text{LBE}}, \tag{2}$$

where $\mathbf{m} = \mathbf{M}(f_i)^{\text{T}}$ is the rescaled moment with $\mathbf{M}$ being the dimensionless transformation matrix [22], and $\bar{\mathbf{m}}$ denotes the post-collision moment. For the sake of simplicity, the two-dimensional nine-velocity (D2Q9) lattice is considered here [23], and the extension to three-dimensional lattice is straightforward though tedious. The equilibrium moment function $\mathbf{m}^{\text{eq}} = \mathbf{M}(f_i^{\text{eq}})^{\text{T}}$ is devised as

$$\mathbf{m}^{\text{eq}} = \big[\rho,\ 2\alpha_1\rho + 2\beta_1\eta + 3\rho|\hat{\mathbf{u}}|^2,\ \alpha_2\rho + \beta_2\eta - 3\rho|\hat{\mathbf{u}}|^2 + 9\rho\hat{u}_x^2\hat{u}_y^2,$$

$$\rho\hat{u}_x,\ -\rho\hat{u}_x + 3\rho\hat{u}_x\hat{u}_y^2,\ \rho\hat{u}_y,\ -\rho\hat{u}_y + 3\rho\hat{u}_y\hat{u}_x^2,\ \rho(\hat{u}_x^2 - \hat{u}_y^2),\ \rho\hat{u}_x\hat{u}_y\big]^{\text{T}}, \tag{3}$$

where $\hat{\mathbf{u}} = \mathbf{u}/c$ with lattice speed $c = \delta_x/\delta_t$, η is introduced to achieve the self-tuning EOS, and $\alpha_{1,2}$ and $\beta_{1,2}$ are coefficients that will be determined later [see Eq. (25)]. The corresponding discrete force term in moment space $\mathbf{F}_m = \mathbf{M}(F_{v,i})^{\text{T}}$ is set as follows:

$$\mathbf{F}_m = \big[0,\ 6\hat{\mathbf{F}}\cdot\hat{\mathbf{u}},\ -6\hat{\mathbf{F}}\cdot\hat{\mathbf{u}} + 9[\![\hat{\mathbf{F}}\hat{\mathbf{u}}\hat{\mathbf{u}}]\!]_{xxyy},\ \hat{F}_x,\ -\hat{F}_x + 3[\![\hat{\mathbf{F}}\hat{\mathbf{u}}\hat{\mathbf{u}}]\!]_{xyy},$$

$$\hat{F}_y,\ -\hat{F}_y + 3[\![\hat{\mathbf{F}}\hat{\mathbf{u}}\hat{\mathbf{u}}]\!]_{xxy},\ 2(\hat{F}_x\hat{u}_x - \hat{F}_y\hat{u}_y),\ \hat{F}_x\hat{u}_y + \hat{F}_y\hat{u}_x\big]^{\text{T}}, \tag{4}$$

where $\hat{\mathbf{F}} = \mathbf{F}/c$, $[\![\cdots]\!]$ denotes permutation (e.g., $[\![\hat{\mathbf{F}}\hat{\mathbf{u}}\hat{\mathbf{u}}]\!] = \hat{\mathbf{F}}\hat{\mathbf{u}}\hat{\mathbf{u}} + \hat{\mathbf{u}}\hat{\mathbf{F}}\hat{\mathbf{u}} + \hat{\mathbf{u}}\hat{\mathbf{u}}\hat{\mathbf{F}}$) and the subscripts denote tensor indices. In Eqs. (3) and (4), the high-order terms of velocity correspond to the third- and fourth-order Hermite terms in f_i^{eq} and $F_{v,i}$, which are necessary to eliminate the additional cubic terms of velocity [20,24]. The macroscopic density ρ and velocity $\mathbf{u}$ are defined as

$$\rho = \sum_i f_i, \quad \rho\mathbf{u} = \sum_i \mathbf{e}_i f_i + \frac{\delta_t}{2}\mathbf{F}. \tag{5}$$

Once the equilibrium distribution function in the LB equation is changed to achieve a self-tuning EOS, Newtonian viscous stress cannot be recovered correctly and Galilean invariance will be lost (as recognized previously [13,25]). From the Enskog equation for dense gases in kinetic theory, we note that an extra velocity-dependent term emerges in the collision term [7,8,26]. Inspired by this fact, some velocity-dependent nondiagonal elements are introduced in the collision matrix $\mathbf{S}$:

$$\mathbf{S} = \begin{bmatrix} s_0 & 0 & 0 & 0 & 0 & 0 & 0 & 0 & 0 \\ 0 & s_e & ks_\varepsilon\omega_e & 0 & h\hat{u}_x s_q\omega_e & 0 & h\hat{u}_y s_q\omega_e & 0 & 0 \\ 0 & 0 & s_\varepsilon & 0 & 0 & 0 & 0 & 0 & 0 \\ 0 & 0 & 0 & s_j & 0 & 0 & 0 & 0 & 0 \\ 0 & 0 & 0 & 0 & s_q & 0 & 0 & 0 & 0 \\ 0 & 0 & 0 & 0 & 0 & s_j & 0 & 0 & 0 \\ 0 & 0 & 0 & 0 & 0 & 0 & s_q & 0 & 0 \\ 0 & 0 & 0 & 0 & 2b\hat{u}_x s_q\omega_p & 0 & -2b\hat{u}_y s_q\omega_p & s_p & 0 \\ 0 & 0 & 0 & 0 & b\hat{u}_y s_q\omega_p & 0 & b\hat{u}_x s_q\omega_p & 0 & s_p \end{bmatrix}, \tag{6}$$

where $\omega_{e,p} = s_{e,p}/2 - 1$, and k, h, and b are coefficients that will be determined via the second-order Chapman-Enskog (CE) analysis [see Eq. (25)]. Note that this improved collision matrix is still invertible, and the inverse matrix $\mathbf{S}^{-1}$ is given in Appendix A.

To entirely eliminate the additional cubic terms of velocity in the recovered macroscopic equation at the Navier-Stokes level, the correction matrices $\mathbf{R}$, $\mathbf{T}$, and $\mathbf{X}$ are set in the following forms [20]:

$$\mathbf{R} = \begin{bmatrix} 0 & 0 & 0 & 0 & 0 & 0 & 0 & 0 & 0 \\ 0 & R_{11} & 0 & 0 & 0 & 0 & 0 & R_{17} & R_{18} \\ 0 & 0 & 0 & 0 & 0 & 0 & 0 & 0 & 0 \\ 0 & 0 & 0 & 0 & 0 & 0 & 0 & 0 & 0 \\ 0 & 0 & 0 & 0 & 0 & 0 & 0 & 0 & 0 \\ 0 & 0 & 0 & 0 & 0 & 0 & 0 & 0 & 0 \\ 0 & 0 & 0 & 0 & 0 & 0 & 0 & 0 & 0 \\ 0 & R_{71} & 0 & 0 & 0 & 0 & 0 & R_{77} & R_{78} \\ 0 & R_{81} & 0 & 0 & 0 & 0 & 0 & R_{87} & R_{88} \end{bmatrix}, \tag{7a}$$

$$\mathbf{T} = [\mathbf{0},\ \mathbf{T}_1,\ \mathbf{0},\ \mathbf{0},\ \mathbf{0},\ \mathbf{0},\ \mathbf{0},\ \mathbf{T}_7,\ \mathbf{T}_8]^{\text{T}}, \tag{7b}$$

$$\mathbf{X} = [\mathbf{0},\ \mathbf{X}_1,\ \mathbf{0},\ \mathbf{0},\ \mathbf{0},\ \mathbf{0},\ \mathbf{0},\ \mathbf{X}_7,\ \mathbf{X}_8]^{\text{T}}, \tag{7c}$$

where the nonzero elements can be uniquely and locally determined via the second-order CE analysis. In Eqs. (7b) and (7c), $\mathbf{T}_{1,7,8}$ and $\mathbf{X}_{1,7,8}$ are vectors, which mean that the dimensions of $\mathbf{T}$ and $\mathbf{X}$ are 9×2. Note that $\mathbf{R}$, $\mathbf{T}$, and $\mathbf{X}$ are of order Ma^2, Ma^3, and Ma^3, respectively, with Ma denoting the lattice Mach number, and thus the corresponding correction terms in LB equation have negligible effects on the numerical stability.

A. Second-order analysis

To determine the coefficients in $\mathbf{m}^{\mathrm{eq}}$ and $\mathbf{S}$, as well as the nonzero elements in $\mathbf{R}$, $\mathbf{T}$, and $\mathbf{X}$, the second-order CE analysis of the above LB model is carried out in this part. For the LB equation [i.e., Eq. (1)], performing Taylor series expansion of $f_i(\mathbf{x} + \mathbf{e}_i \delta_t, t + \delta_t)$ centered at $(\mathbf{x}, t)$, and then transforming the result into moment space, we can obtain

$$(\mathbf{I}\partial_t + \mathbf{D})\mathbf{m} + \frac{\delta_t}{2}(\mathbf{I}\partial_t + \mathbf{D})^2 \mathbf{m}$$

$$+ \frac{\delta_t^2}{6}(\mathbf{I}\partial_t + \mathbf{D})^3 \mathbf{m} - \mathbf{F}_m + O(\delta_t^3)$$

$$= -\left[\frac{\mathbf{S}}{\delta_t} + \frac{\mathbf{R}}{\delta_t}\left(\mathbf{I} - \frac{\mathbf{S}}{2}\right)\right]\left(\mathbf{m} - \mathbf{m}^{\mathrm{eq}} + \frac{\delta_t}{2}\mathbf{F}_m\right)$$

$$- \frac{\delta_x \mathbf{T}}{\delta_t} \cdot \nabla \rho - \frac{\delta_x \mathbf{X}}{c^2 \delta_t} \cdot \nabla p_{\mathrm{LBE}}, \qquad (8)$$

where $\mathbf{D} = \mathbf{M}[\mathrm{diag}(\mathbf{e}_i \cdot \nabla)]\mathbf{M}^{-1}$. In this work, the following classical CE expansions are adopted [26]:

$$\partial_t = \sum_{n=1}^{+\infty} \varepsilon^n \partial_{tn}, \quad \nabla = \varepsilon^1 \nabla_1,$$

$$f_i = \sum_{n=0}^{+\infty} \varepsilon^n f_i^{(n)}, \quad \mathbf{F} = \varepsilon^1 \mathbf{F}^{(1)}, \qquad (9a)$$

which indicate

$$\mathbf{D} = \varepsilon^1 \mathbf{D}_1, \quad \mathbf{m} = \sum_{n=0}^{+\infty} \varepsilon^n \mathbf{m}^{(n)}, \quad \mathbf{F}_m = \varepsilon^1 \mathbf{F}_m^{(1)}. \qquad (9b)$$

Here, ε is the small expansion parameter. Substituting the above expansions into Eq. (8), we can rewrite Eq. (8) in the consecutive orders of ε as follows:

$$\varepsilon^0: \ -\frac{\mathbf{S}}{\delta_t}(\mathbf{m}^{(0)} - \mathbf{m}^{\mathrm{eq}}) - \frac{\mathbf{R}}{\delta_t}\left(\mathbf{I} - \frac{\mathbf{S}}{2}\right)(\mathbf{m}^{(0)} - \mathbf{m}^{\mathrm{eq}}) = \mathbf{0}, \qquad (10a)$$

$$\varepsilon^1: \ (\mathbf{I}\partial_{t1} + \mathbf{D}_1)\mathbf{m}^{(0)} - \mathbf{F}_m^{(1)} = -\frac{\mathbf{S}}{\delta_t}\mathbf{G}^{(1)} + \frac{2}{\delta_t}(\tilde{\mathbf{G}}^{(1)} - \hat{\mathbf{G}}^{(1)}), \qquad (10b)$$

$$\varepsilon^2: \ \partial_{t2}\mathbf{m}^{(0)} + (\mathbf{I}\partial_{t1} + \mathbf{D}_1)\tilde{\mathbf{G}}^{(1)} = -\frac{\mathbf{S}}{\delta_t}\mathbf{m}^{(2)} - \frac{\mathbf{R}}{\delta_t}\left(\mathbf{I} - \frac{\mathbf{S}}{2}\right)\mathbf{m}^{(2)}, \qquad (10c)$$

where $\mathbf{G}^{(1)} = \mathbf{m}^{(1)} + \delta_t/2 \, \mathbf{F}_m^{(1)}$, $\hat{\mathbf{G}}^{(1)} = (\mathbf{I} - \mathbf{S}/2)\mathbf{G}^{(1)}$, and $\tilde{\mathbf{G}}^{(1)} = (\mathbf{I} - \mathbf{R}/2)\hat{\mathbf{G}}^{(1)} - \delta_x \mathbf{T}/2 \cdot \nabla_1 \rho - \delta_x \mathbf{X}/(2c^2) \cdot \nabla_1 p_{\mathrm{LBE}}$ are introduced to simplify the descriptions.

Based on the ε^0-order equation [i.e., Eq. (10a)], we have

$$\varepsilon^0: \ \mathbf{m}^{(0)} = \mathbf{m}^{\mathrm{eq}}, \qquad (11)$$

which further indicates that

$$\begin{cases} \tilde{G}_0^{(1)} = \hat{G}_0^{(1)} = G_0^{(1)} = 0, & m_0^{(n)} = 0 \ (\forall n \geqslant 2), \\ \tilde{G}_3^{(1)} = \hat{G}_3^{(1)} = G_3^{(1)} = 0, & m_3^{(n)} = 0 \ (\forall n \geqslant 2), \\ \tilde{G}_5^{(1)} = \hat{G}_5^{(1)} = G_5^{(1)} = 0, & m_5^{(n)} = 0 \ (\forall n \geqslant 2), \end{cases} \qquad (12)$$

by considering Eq. (5). Extracting the ε^1-order equations for the conserved moments m_0, m_3, and m_5 from Eq. (10b) and considering Eqs. (11) and (12), the following macroscopic equation can be obtained:

$$\varepsilon^1: \begin{cases} \partial_{t1}\rho + \nabla_1 \cdot (\rho \mathbf{u}) = 0, \\ \partial_{t1}(\rho \mathbf{u}) + \nabla_1 \cdot (\rho \mathbf{u}\mathbf{u}) = -\nabla_1 p_{\mathrm{LBE}} + \mathbf{F}^{(1)}, \end{cases} \qquad (13)$$

where the directly recovered EOS p_{LBE} is

$$p_{\mathrm{LBE}} = c_s^2[(2 + \alpha_1)\rho + \beta_1 \eta], \qquad (14)$$

and $c_s = c/\sqrt{3}$ is the lattice sound speed. Similarly, extracting the ε^2-order equations for m_0, m_3, and m_5 from Eq. (10c) and considering Eqs. (11) and (12), we have

$$\varepsilon^2: \begin{cases} \partial_{t2}\rho = 0, \\ \partial_{t2}(\rho \mathbf{u}) = \nabla_1 \cdot \mathbf{\Pi}^{(1)}, \end{cases} \qquad (15)$$

where the viscous stress tensor $\mathbf{\Pi}^{(1)}$ is generally expressed as

$$\mathbf{\Pi}^{(1)} = -c^2 \begin{bmatrix} \frac{1}{2}\tilde{G}_7^{(1)} & \tilde{G}_8^{(1)} \\ \tilde{G}_8^{(1)} & -\frac{1}{2}\tilde{G}_7^{(1)} \end{bmatrix} - c^2 \begin{bmatrix} \frac{1}{6}\tilde{G}_1^{(1)} & 0 \\ 0 & \frac{1}{6}\tilde{G}_1^{(1)} \end{bmatrix}. \qquad (16)$$

1. Newtonian viscous stress

To calculate the viscous stress tensor given by Eq. (16), the equations for the related moments (m_1, m_7, and m_8) at the order of ε^1 are extracted from Eq. (10b) as follows:

$$-\frac{1}{\delta_t}\left(s_e G_1^{(1)} + k s_\varepsilon \omega_e G_2^{(1)} + h \hat{u}_x s_q \omega_e G_4^{(1)} + h \hat{u}_y s_q \omega_e G_6^{(1)}\right) + \frac{2}{\delta_t}\left(\tilde{G}_1^{(1)} - \hat{G}_1^{(1)}\right)$$

$$= \partial_{t1}m_1^{(0)} + c\partial_{x1}\left(m_3^{(0)} + m_4^{(0)}\right) + c\partial_{y1}\left(m_5^{(0)} + m_6^{(0)}\right) - F_{m,1}^{(1)}, \qquad (17a)$$

$$-\frac{1}{\delta_t}\left(s_p G_7^{(1)} + 2b\hat{u}_x s_q \omega_p G_4^{(1)} - 2b\hat{u}_y s_q \omega_p G_6^{(1)}\right) + \frac{2}{\delta_t}\left(\tilde{G}_7^{(1)} - \hat{G}_7^{(1)}\right)$$

$$= \partial_{t1}m_7^{(0)} + c\partial_{x1}\left(\frac{1}{3}m_3^{(0)} - \frac{1}{3}m_4^{(0)}\right) - c\partial_{y1}\left(\frac{1}{3}m_5^{(0)} - \frac{1}{3}m_6^{(0)}\right) - F_{m,7}^{(1)}, \qquad (17b)$$

$$
-\frac{1}{\delta_t}\left(s_p G_8^{(1)} + b\hat{u}_y s_q \omega_p G_4^{(1)} + b\hat{u}_x s_q \omega_p G_6^{(1)}\right) + \frac{2}{\delta_t}\left(\tilde{G}_8^{(1)} - \hat{G}_8^{(1)}\right)
$$

$$
= \partial_{t1} m_8^{(0)} + c\partial_{x1}\left(\frac{2}{3}m_5^{(0)} + \frac{1}{3}m_6^{(0)}\right) + c\partial_{y1}\left(\frac{2}{3}m_3^{(0)} + \frac{1}{3}m_4^{(0)}\right) - F_{m,8}^{(1)}, \tag{17c}
$$

where the involved ε^1-order terms $G_2^{(1)}$, $G_4^{(1)}$, and $G_6^{(1)}$ can also be obtained from Eq. (10b)

$$
-\frac{1}{\delta_t}s_\varepsilon G_2^{(1)} = \partial_{t1} m_2^{(0)} + c\partial_{x1} m_4^{(0)} + c\partial_{y1} m_6^{(0)} - F_{m,2}^{(1)}, \tag{18a}
$$

$$
-\frac{1}{\delta_t}s_q G_4^{(1)} = \partial_{t1} m_4^{(0)} + c\partial_{x1}\left(\frac{1}{3}m_1^{(0)} + \frac{1}{3}m_2^{(0)} - m_7^{(0)}\right) + c\partial_{y1} m_8^{(0)} - F_{m,4}^{(1)}, \tag{18b}
$$

$$
-\frac{1}{\delta_t}s_q G_6^{(1)} = \partial_{t1} m_6^{(0)} + c\partial_{x1} m_8^{(0)} + c\partial_{y1}\left(\frac{1}{3}m_1^{(0)} + \frac{1}{3}m_2^{(0)} + m_7^{(0)}\right) - F_{m,6}^{(1)}. \tag{18c}
$$

Multiplying Eqs. (18a), (18b), and (18c) by k, $h\hat{u}_x$, and $h\hat{u}_y$, respectively, and then adding the results to Eq. (17a), the following relation can be obtained after lengthy algebra:

$$
-\frac{1}{\delta_t}\frac{2s_e}{2-s_e}\hat{G}_1^{(1)} + \frac{2}{\delta_t}\left(\tilde{G}_1^{(1)} - \hat{G}_1^{(1)}\right)
$$

$$
= -(2\alpha_1 + k\alpha_2 + k)\nabla_1 \cdot (\rho\mathbf{u}) + \frac{h[(\alpha_2 - 4)\beta_1 - (\alpha_1 + 2)\beta_2]}{3\beta_1}\mathbf{u}\cdot\nabla_1\rho + \frac{h(3\beta_1 + \beta_2) - 6\beta_1(1-k)}{\beta_1}\mathbf{u}\cdot\nabla_1\hat{p}_{\text{LBE}} + (2\beta_1 + k\beta_2)\partial_{t1}\eta
$$

$$
- c\left\{9(2k+h)\hat{u}_x\hat{u}_y^2\partial_{x1}\hat{p}_{\text{LBE}} + 9(2k+h)\hat{u}_x^2\hat{u}_y\partial_{y1}\hat{p}_{\text{LBE}}\right\}
$$

$$
- c\left\{3\left[(1-k)\hat{u}_x^3 - (2k+h)\hat{u}_x\hat{u}_y^2\right]\partial_{x1}\rho + 3\left[(1-k)\hat{u}_y^3 - (2k+h)\hat{u}_x^2\hat{u}_y\right]\partial_{y1}\rho\right\}
$$

$$
- c\left\{\left[9(1-k)\hat{u}_x^2 - 2(3k+h)\hat{u}_y^2\right]\rho\partial_{x1}\hat{u}_x + \left[9(1-k)\hat{u}_y^2 - 2(3k+h)\hat{u}_x^2\right]\rho\partial_{y1}\hat{u}_y - 4(3k+h)\hat{u}_x\hat{u}_y\rho(\partial_{x1}\hat{u}_y + \partial_{y1}\hat{u}_x)\right\}
$$

$$
- c\left\{9k\nabla_1 \cdot \left(\rho\hat{\mathbf{u}}\hat{u}_x^2\hat{u}_y^2\right) + 3h\hat{u}_y\partial_{x1}\left(\rho\hat{u}_x^3\hat{u}_y\right) + 3h\hat{u}_x\partial_{y1}\left(\rho\hat{u}_x\hat{u}_y^3\right)\right\}, \tag{19}
$$

where $\hat{p}_{\text{LBE}} = p_{\text{LBE}}/c^2$. To correctly recover the Newtonian viscous stress, one should have

$$
\begin{cases}
2\alpha_1 + k\alpha_2 + k = \frac{h[(\alpha_2-4)\beta_1-(\alpha_1+2)\beta_2]}{3\beta_1} \equiv -2\varpi, \\
\frac{h(3\beta_1+\beta_2)-6\beta_1(1-k)}{\beta_1} = 0, \\
2\beta_1 + k\beta_2 = 0.
\end{cases} \tag{20}
$$

Here, a crucial parameter ϖ is further introduced, and it is worth emphasizing that ϖ cannot be simply set to 1 following the classical LB model with ideal-gas EOS. Otherwise, a singularity will be encountered [see Eq. (25)] and the present model should degenerate into the classical LB model. Moreover, there exist some third- and fifth-order additional terms of velocity in Eq. (19), which can be simply ignored under the low Mach number condition. As a better choice, eliminating the third-order terms (i.e., cubic terms) will be discussed later.

Multiplying Eqs. (18b) and (18c) by $2b\hat{u}_x$ and $-2b\hat{u}_y$, respectively, and then adding the results to Eq. (17b), the following relation can be finally obtained:

$$
-\frac{1}{\delta_t}\frac{2s_p}{2-s_p}\hat{G}_7^{(1)} + \frac{2}{\delta_t}\left(\tilde{G}_7^{(1)} - \hat{G}_7^{(1)}\right)
$$

$$
= \frac{2}{3}[\partial_{x1}(\rho u_x) - \partial_{y1}(\rho u_y)] + \frac{2}{3}\frac{b[(\alpha_2-4)\beta_1-(\alpha_1+2)\beta_2]}{\beta_1}(u_x\partial_{x1}\rho - u_y\partial_{y1}\rho) + \frac{(6b-2)\beta_1+2b\beta_2}{\beta_1}(u_x\partial_{x1}\hat{p}_{\text{LBE}} - u_y\partial_{y1}\hat{p}_{\text{LBE}})
$$

$$
+ c\left\{6b\hat{u}_x\hat{u}_y^2\partial_{x1}\hat{p}_{\text{LBE}} - 6b\hat{u}_x^2\hat{u}_y\partial_{y1}\hat{p}_{\text{LBE}}\right\} - c\left\{\left(\hat{u}_x^3 + 2b\hat{u}_x\hat{u}_y^2\right)\partial_{x1}\rho - \left(\hat{u}_y^3 + 2b\hat{u}_x^2\hat{u}_y\right)\partial_{y1}\rho\right\}
$$

$$
- c\left\{\left(3\hat{u}_x^2 + 4b\hat{u}_y^2\right)\rho\partial_{x1}\hat{u}_x - \left(3\hat{u}_y^2 + 4b\hat{u}_x^2\right)\rho\partial_{y1}\hat{u}_y\right\} + c\left\{6b\hat{u}_y\partial_{x1}\left(\rho\hat{u}_x^3\hat{u}_y\right) - 6b\hat{u}_x\partial_{y1}\left(\rho\hat{u}_x\hat{u}_y^3\right)\right\}. \tag{21}
$$

To correctly recover the Newtonian viscous stress, one should have

$$
\begin{cases}
\frac{b[(\alpha_2-4)\beta_1-(\alpha_1+2)\beta_2]}{\beta_1} = -1, \\
\frac{(6b-2)\beta_1+2b\beta_2}{\beta_1} = 0.
\end{cases} \tag{22}
$$

Multiplying Eqs. (18b) and (18c) by $b\hat{u}_y$ and $b\hat{u}_x$, respectively, and then adding the results to Eq. (17c), the following relation can be obtained:

$$
-\frac{1}{\delta_t}\frac{2s_p}{2-s_p}\hat{G}_8^{(1)} + \frac{2}{\delta_t}\left(\tilde{G}_8^{(1)} - \hat{G}_8^{(1)}\right)
$$

$$
= \frac{1}{3}[\partial_{x1}(\rho u_y) + \partial_{y1}(\rho u_x)] + \frac{1}{3}\frac{b[(\alpha_2 - 4)\beta_1 - (\alpha_1 + 2)\beta_2]}{\beta_1}(u_y\partial_{x1}\rho + u_x\partial_{y1}\rho) + \frac{(3b-1)\beta_1 + b\beta_2}{\beta_1}(u_y\partial_{x1}\hat{p}_{\mathrm{LBE}} + u_x\partial_{y1}\hat{p}_{\mathrm{LBE}})
$$

$$
- c\left\{3b(\hat{u}_y^3 + 2\hat{u}_x^2\hat{u}_y)\partial_{x1}\hat{p}_{\mathrm{LBE}} + 3b(\hat{u}_x^3 + 2\hat{u}_x\hat{u}_y^2)\partial_{y1}\hat{p}_{\mathrm{LBE}}\right\} + c\left\{b(\hat{u}_y^3 + 2\hat{u}_x^2\hat{u}_y)\partial_{x1}\rho + b(\hat{u}_x^3 + 2\hat{u}_x\hat{u}_y^2)\partial_{y1}\rho\right\}
$$

$$
+ c\left\{2b\hat{u}_x\hat{u}_y\rho\partial_{x1}\hat{u}_x + 2b\hat{u}_x\hat{u}_y\rho\partial_{y1}\hat{u}_y + 2b(\hat{u}_x^2 + \hat{u}_y^2)\rho(\partial_{x1}\hat{u}_y + \partial_{y1}\hat{u}_x)\right\} - c\left\{3b\hat{u}_x\partial_{x1}(\rho\hat{u}_x^3\hat{u}_y) + 3b\hat{u}_y\partial_{y1}(\rho\hat{u}_x\hat{u}_y^3)\right\}. \quad (23)
$$

Similarly, to correctly recover the Newtonian viscous stress, one should have

$$
\begin{cases}
\frac{b[(\alpha_2 - 4)\beta_1 - (\alpha_1 + 2)\beta_2]}{\beta_1} = -1, \\
\frac{(3b-1)\beta_1 + b\beta_2}{\beta_1} = 0.
\end{cases} \quad (24)
$$

Here, we note that Eq. (24) is actually the same as Eq. (22), which indicates that the diagonal and non-diagonal elements in the traceless part of viscous stress tensor can be correctly recovered, or not, at the same time.

Equations (20), (22), and (24) give the constraints on the coefficients in $\mathbf{m}^{\mathrm{eq}}$ and $\mathbf{S}$ required for the correct recovery of Newtonian viscous stress. Considering that the classical LB model can be viewed as a special case of the present LB model, Eqs. (20), (22), and (24) must be compatible with each other. Solving these equations, we have

$$
\alpha_2 = -\frac{2\alpha_1 + \varpi + 1}{1 - \varpi}, \quad \beta_2 = -\frac{2\beta_1}{1 - \varpi}, \quad k = 1 - \varpi, \quad h = \frac{6\varpi(1 - \varpi)}{1 - 3\varpi}, \quad b = \frac{1 - \varpi}{1 - 3\varpi}. \quad (25)
$$

In practical applications, α_1 is set to -1 according to the ordinary equilibrium moment function derived from the Maxwell-Boltzmann distribution, and β_1 is set to 1 as usual. Therefore, all the coefficients α_2, β_2, k, h, and b are uniquely determined by ϖ.

2. Cubic terms of velocity

From Eqs. (19), (21), and (23), and considering $\mathbf{R} \sim O(\mathrm{Ma}^2)$, $\mathbf{T} \sim O(\mathrm{Ma}^3)$, and $\mathbf{X} \sim O(\mathrm{Ma}^3)$, we have $\hat{G}_1^{(1)} \sim O(\mathrm{Ma})$, $\hat{G}_7^{(1)} \sim O(\mathrm{Ma})$, and $\hat{G}_8^{(1)} \sim O(\mathrm{Ma})$. Thus, the leading-order terms of Eqs. (19), (21), and (23) can be given as

$$
\begin{cases}
-\frac{1}{\delta_t}\frac{2s_e}{2-s_e}\hat{G}_1^{(1)} = 2\varpi\rho(\partial_{x1}u_x + \partial_{y1}u_y) + O(\mathrm{Ma}^3), \\
-\frac{1}{\delta_t}\frac{2s_p}{2-s_p}\hat{G}_7^{(1)} = \frac{2}{3}\rho(\partial_{x1}u_x - \partial_{y1}u_y) + O(\mathrm{Ma}^3), \\
-\frac{1}{\delta_t}\frac{2s_p}{2-s_p}\hat{G}_8^{(1)} = \frac{1}{3}\rho(\partial_{x1}u_y + \partial_{y1}u_x) + O(\mathrm{Ma}^3).
\end{cases} \quad (26)
$$

Based on Eq. (19) and $\tilde{G}_1^{(1)} = \hat{G}_1^{(1)} - \frac{1}{2}(R_{11}\hat{G}_1^{(1)} + R_{17}\hat{G}_7^{(1)} + R_{18}\hat{G}_8^{(1)} + \delta_x\mathbf{T}_1 \cdot \boldsymbol{\nabla}_1\rho + \delta_x\mathbf{X}_1 \cdot \boldsymbol{\nabla}_1\hat{p}_{\mathrm{LBE}})$, we have

$$
-\frac{1}{\delta_t}\frac{2s_e}{2-s_e}\tilde{G}_1^{(1)} = 2\varpi\rho(\partial_{x1}u_x + \partial_{y1}u_y) + \frac{1}{\delta_t}\frac{2}{2-s_e}\left(R_{11}\hat{G}_1^{(1)} + R_{17}\hat{G}_7^{(1)} + R_{18}\hat{G}_8^{(1)} + \delta_x\mathbf{T}_1 \cdot \boldsymbol{\nabla}_1\rho + \delta_x\mathbf{X}_1 \cdot \boldsymbol{\nabla}_1\hat{p}_{\mathrm{LBE}}\right)
$$

$$
- c\left\{9(2k + h)\hat{u}_x\hat{u}_y^2\partial_{x1}\hat{p}_{\mathrm{LBE}} + 9(2k + h)\hat{u}_x^2\hat{u}_y\partial_{y1}\hat{p}_{\mathrm{LBE}}\right\}
$$

$$
- c\left\{3[(1 - k)\hat{u}_x^3 - (2k + h)\hat{u}_x\hat{u}_y^2]\partial_{x1}\rho + 3[(1 - k)\hat{u}_y^3 - (2k + h)\hat{u}_x^2\hat{u}_y]\partial_{y1}\rho\right\}
$$

$$
- c\left\{\begin{array}{l}[9(1 - k)\hat{u}_x^2 - 2(3k + h)\hat{u}_y^2]\rho\partial_{x1}\hat{u}_x + [9(1 - k)\hat{u}_y^2 - 2(3k + h)\hat{u}_x^2]\rho\partial_{y1}\hat{u}_y \\ -4(3k + h)\hat{u}_x\hat{u}_y\rho(\partial_{x1}\hat{u}_y + \partial_{y1}\hat{u}_x)\end{array}\right\}
$$

$$
- c\left\{9k\boldsymbol{\nabla}_1 \cdot (\rho\hat{\mathbf{u}}\hat{u}_x^2\hat{u}_y^2) + 3h\hat{u}_y\partial_{x1}(\rho\hat{u}_x^3\hat{u}_y) + 3h\hat{u}_x\partial_{y1}(\rho\hat{u}_x\hat{u}_y^3)\right\}. \quad (27)
$$

To eliminate the additional cubic terms of velocity in Eq. (27) and with the consideration of Eq. (26), we can set

$$
R_{11} = -\frac{(9 - 15k - 2h)s_e}{4\varpi}(\hat{u}_x^2 + \hat{u}_y^2), \quad R_{17} = -\frac{3(9 - 3k + 2h)s_p(2 - s_e)}{4(2 - s_p)}(\hat{u}_x^2 - \hat{u}_y^2), \quad R_{18} = \frac{12(3k + h)s_p(2 - s_e)}{2 - s_p}\hat{u}_x\hat{u}_y,
$$

$$
\mathbf{T}_1 = \frac{3(2 - s_e)}{2}\begin{bmatrix}(1 - k)\hat{u}_x^3 - (2k + h)\hat{u}_x\hat{u}_y^2 \\ (1 - k)\hat{u}_y^3 - (2k + h)\hat{u}_x^2\hat{u}_y\end{bmatrix}, \quad \mathbf{X}_1 = \frac{9(2k + h)(2 - s_e)}{2}\begin{bmatrix}\hat{u}_x\hat{u}_y^2 \\ \hat{u}_x^2\hat{u}_y\end{bmatrix}. \quad (28)
$$

Thus, Eq. (27) can be finally simplified as

$$
-\frac{1}{\delta_t}\frac{2s_e}{2-s_e}\tilde{G}_1^{(1)} = 2\varpi\rho(\partial_{x1}u_x + \partial_{y1}u_y) + O(\mathrm{Ma}^5). \quad (29)
$$

From Eq. (21), and considering $\tilde{G}_7^{(1)} = \hat{G}_7^{(1)} - \frac{1}{2}(R_{71}\hat{G}_1^{(1)} + R_{77}\hat{G}_7^{(1)} + R_{78}\hat{G}_8^{(1)} + \delta_x \mathbf{T}_7 \cdot \boldsymbol{\nabla}_1 \rho + \delta_x \mathbf{X}_7 \cdot \boldsymbol{\nabla}_1 \hat{p}_{\text{LBE}})$, we have

$$
\begin{aligned}
-\frac{1}{\delta_t}\frac{2s_p}{2-s_p}\tilde{G}_7^{(1)} &= \frac{2}{3}\rho(\partial_{x1}u_x - \partial_{y1}u_y) + \frac{1}{\delta_t}\frac{2}{2-s_p}\big(R_{71}\hat{G}_1^{(1)} + R_{77}\hat{G}_7^{(1)} + R_{78}\hat{G}_8^{(1)} + \delta_x\mathbf{T}_7 \cdot \boldsymbol{\nabla}_1\rho + \delta_x\mathbf{X}_7 \cdot \boldsymbol{\nabla}_1\hat{p}_{\text{LBE}}\big) \\
&\quad + c\big\{6b\hat{u}_x\hat{u}_y^2\partial_{x1}\hat{p}_{\text{LBE}} - 6b\hat{u}_x^2\hat{u}_y\partial_{y1}\hat{p}_{\text{LBE}}\big\} - c\big\{\big(\hat{u}_x^3 + 2b\hat{u}_x\hat{u}_y^2\big)\partial_{x1}\rho - \big(\hat{u}_y^3 + 2b\hat{u}_x^2\hat{u}_y\big)\partial_{y1}\rho\big\} \\
&\quad - c\big\{\big(3\hat{u}_x^2 + 4b\hat{u}_y^2\big)\rho\partial_{x1}\hat{u}_x - \big(3\hat{u}_y^2 + 4b\hat{u}_x^2\big)\rho\partial_{y1}\hat{u}_y\big\} + c\big\{6b\hat{u}_y\partial_{x1}\big(\rho\hat{u}_x^2\hat{u}_y\big) - 6b\hat{u}_x\partial_{y1}\big(\rho\hat{u}_x\hat{u}_y^3\big)\big\}. \quad (30)
\end{aligned}
$$

To eliminate the additional cubic terms of velocity in Eq. (30) and with the consideration of Eq. (26), we can set

$$
R_{71} = -\frac{(3-4b)s_e(2-s_p)}{4\varpi(2-s_e)}\big(\hat{u}_x^2 - \hat{u}_y^2\big), \quad R_{77} = -\frac{3(3+4b)s_p}{4}\big(\hat{u}_x^2 + \hat{u}_y^2\big), \quad R_{78} = 0,
$$

$$
\mathbf{T}_7 = \frac{2-s_p}{2}\begin{bmatrix} \hat{u}_x^3 + 2b\hat{u}_x\hat{u}_y^2 \\ -\hat{u}_y^3 - 2b\hat{u}_x^2\hat{u}_y \end{bmatrix}, \quad \mathbf{X}_7 = -3b(2-s_p)\begin{bmatrix} \hat{u}_x\hat{u}_y^2 \\ -\hat{u}_x^2\hat{u}_y \end{bmatrix}. \quad (31)
$$

Thus, Eq. (30) is finally simplified as

$$
-\frac{1}{\delta_t}\frac{2s_p}{2-s_p}\tilde{G}_7^{(1)} = \frac{2}{3}\rho(\partial_{x1}u_x - \partial_{y1}u_y) + O(\text{Ma}^5). \quad (32)
$$

Based on Eq. (23), and considering $\tilde{G}_8^{(1)} = \hat{G}_8^{(1)} - \frac{1}{2}(R_{81}\hat{G}_1^{(1)} + R_{87}\hat{G}_7^{(1)} + R_{88}\hat{G}_8^{(1)} + \delta_x \mathbf{T}_8 \cdot \boldsymbol{\nabla}_1 \rho + \delta_x \mathbf{X}_8 \cdot \boldsymbol{\nabla}_1 \hat{p}_{\text{LBE}})$, we have

$$
\begin{aligned}
-\frac{1}{\delta_t}\frac{2s_p}{2-s_p}\tilde{G}_8^{(1)} &= \frac{1}{3}\rho(\partial_{x1}u_y + \partial_{y1}u_x) + \frac{1}{\delta_t}\frac{2}{2-s_p}\big(R_{81}\hat{G}_1^{(1)} + R_{87}\hat{G}_7^{(1)} + R_{88}\hat{G}_8^{(1)} + \delta_x\mathbf{T}_8 \cdot \boldsymbol{\nabla}_1\rho + \delta_x\mathbf{X}_8 \cdot \boldsymbol{\nabla}_1\hat{p}_{\text{LBE}}\big) \\
&\quad - c\big\{3b\big(\hat{u}_y^3 + 2\hat{u}_x^2\hat{u}_y\big)\partial_{x1}\hat{p}_{\text{LBE}} + 3b\big(\hat{u}_x^3 + 2\hat{u}_x\hat{u}_y^2\big)\partial_{y1}\hat{p}_{\text{LBE}}\big\} \\
&\quad + c\big\{b\big(\hat{u}_y^3 + 2\hat{u}_x^2\hat{u}_y\big)\partial_{x1}\rho + b\big(\hat{u}_x^3 + 2\hat{u}_x\hat{u}_y^2\big)\partial_{y1}\rho\big\} \\
&\quad + c\big\{2b\hat{u}_x\hat{u}_y\rho\partial_{x1}\hat{u}_x + 2b\hat{u}_x\hat{u}_y\rho\partial_{y1}\hat{u}_y + 2b\big(\hat{u}_x^2 + \hat{u}_y^2\big)\rho(\partial_{x1}\hat{u}_y + \partial_{y1}\hat{u}_x)\big\} \\
&\quad - c\big\{3b\hat{u}_x\partial_{x1}\big(\rho\hat{u}_x^3\hat{u}_y\big) + 3b\hat{u}_y\partial_{y1}\big(\rho\hat{u}_x\hat{u}_y^3\big)\big\}. \quad (33)
\end{aligned}
$$

Similarly, to eliminate the additional cubic terms of velocity, we can set

$$
R_{81} = \frac{bs_e(2-s_p)}{\varpi(2-s_e)}\hat{u}_x\hat{u}_y, \quad R_{87} = 0, \quad R_{88} = 6bs_p\big(\hat{u}_x^2 + \hat{u}_y^2\big),
$$

$$
\mathbf{T}_8 = -\frac{b(2-s_p)}{2}\begin{bmatrix} \hat{u}_y^3 + 2\hat{u}_x^2\hat{u}_y \\ \hat{u}_x^3 + 2\hat{u}_x\hat{u}_y^2 \end{bmatrix}, \quad \mathbf{X}_8 = \frac{3b(2-s_p)}{2}\begin{bmatrix} \hat{u}_y^3 + 2\hat{u}_x^2\hat{u}_y \\ \hat{u}_x^3 + 2\hat{u}_x\hat{u}_y^2 \end{bmatrix}, \quad (34)
$$

and then Eq. (33) is simplified as

$$
-\frac{1}{\delta_t}\frac{2s_p}{2-s_p}\tilde{G}_8^{(1)} = \frac{1}{3}\rho(\partial_{x1}u_y + \partial_{y1}u_x) + O(\text{Ma}^5). \quad (35)
$$

As given by Eqs. (28), (31), and (34), the nonzero elements in $\mathbf{R}$, $\mathbf{T}$, and $\mathbf{X}$ can be uniquely and locally determined, and the results are also consistent with the aforementioned conditions $\mathbf{R} \sim O(\text{Ma}^2)$, $\mathbf{T} \sim O(\text{Ma}^3)$, and $\mathbf{X} \sim O(\text{Ma}^3)$. Based on Eqs. (29), (32), and (35), the viscous stress tensor given by Eq. (16) can be simplified as

$$
\boldsymbol{\Pi}^{(1)} = \rho\nu[\boldsymbol{\nabla}_1\mathbf{u} + \mathbf{u}\boldsymbol{\nabla}_1 - (\boldsymbol{\nabla}_1 \cdot \mathbf{u})\mathbf{I}] + \rho\varsigma(\boldsymbol{\nabla}_1 \cdot \mathbf{u})\mathbf{I} + O(\text{Ma}^5), \quad (36)
$$

where the kinematic viscosity ν and bulk viscosity ς are given as

$$
\nu = c_s^2\big(s_p^{-1} - 1/2\big)\delta_t, \qquad \varsigma = \varpi c_s^2\big(s_e^{-1} - 1/2\big)\delta_t. \quad (37)
$$

3. Macroscopic equation

Combining Eqs. (13) and (15), and utilizing Eq. (36), the macroscopic equation at the Navier-Stokes level can be finally recovered as follows:

$$
\begin{cases} \partial_t\rho + \boldsymbol{\nabla} \cdot (\rho\mathbf{u}) = 0, \\ \partial_t(\rho\mathbf{u}) + \boldsymbol{\nabla} \cdot (\rho\mathbf{u}\mathbf{u}) = -\boldsymbol{\nabla}p_{\text{LBE}} + \mathbf{F} + \boldsymbol{\nabla} \cdot \{\rho\nu[\boldsymbol{\nabla}\mathbf{u} + \mathbf{u}\boldsymbol{\nabla} - (\boldsymbol{\nabla} \cdot \mathbf{u})\mathbf{I}] + \rho\varsigma(\boldsymbol{\nabla} \cdot \mathbf{u})\mathbf{I}\} + O(\text{Ma}^5). \end{cases} \quad (38)
$$

Obviously, the Newtonian viscous stress is correctly recovered and thus the Galilean invariance can be satisfied. In addition, the EOS p_{LBE} directly recovered by the LB equation can be self-tuned via the built-in η [see Eq. (14)]. From the above second-order

analysis, it can also be seen that the force term $\mathbf{F}$ can be recovered with no discrete lattice effect at the ε^2 order.

Before proceeding further, some discussion on the present LB model with self-tuning EOS is useful. For the coefficients $\alpha_{1,2}$ and $\beta_{1,2}$, $\alpha_1 = -1$ and $\beta_1 = 1$ are set as usual, and one has $\alpha_2 = 1$. Therefore, $\mathbf{m}^{\text{eq}}$ given by Eq. (3) can be decomposed into the ordinary one derived from the Hermite expansion of the Maxwell-Boltzmann distribution and the extra one related to η. The coefficient ϖ plays an important role here. When $\varpi = 1$, one has $\beta_2 \to \infty$, $k = 0$, $h = 0$, and $b = 0$. Thus, η should be set to 0 to avoid a singularity, implying that the present model degenerates into the classical LB model with ideal-gas EOS. When $\varpi = 1/3$, one has $\beta_2 = -3$, $k = 2/3$, $h \to \infty$, and $b \to \infty$. Thus, the velocity-dependent terms in $\mathbf{S}$ should be removed to avoid a singularity, which means that Newtonian viscous stress cannot be recovered and Galilean invariance is lost. Compared with previous LB models derived from the Enskog equation via systematic discretization procedures [6–8], the present model is directly constructed at the discrete level in moment space and thus is free of complicated derivative terms, which trigger numerical instability and restrict real applications of previous models [18,19].

III. APPLICATION TO MULTIPHASE FLOWS

As analyzed by He and Doolen [8], a thermodynamically consistent kinetic model for multiphase flows can be established by combining Enskog theory for dense gases and mean-field theory for long-range molecular interaction. In the Enskog equation, short-range molecular interaction (i.e., the effect of molecular volume) is considered by the collision term, and consequently, a nonideal-gas EOS is recovered [26]. From this viewpoint, the present LB model with self-tuning EOS can be interpreted as the incorporation of short-range molecular interaction, and thus the long-range molecular interaction remains to be included to construct a valid model for multiphase flows. Following the idea of the pseudopotential LB model [4,9], a pairwise interaction force is introduced to mimic the long-range molecular interaction. Here, nearest-neighbor interaction is considered, and the interaction force is given as

$$\mathbf{F}(\mathbf{x}) = G^2 \rho(\mathbf{x}) \sum_i \omega(|\mathbf{e}_i \delta_t|^2) \rho(\mathbf{x} + \mathbf{e}_i \delta_t) \mathbf{e}_i \delta_t, \quad (39)$$

where G^2 is used to control the interaction strength, and the weights $\omega(\delta_x^2) = 1/3$ and $\omega(2\delta_x^2) = 1/12$ maximize the isotropy degree of $\mathbf{F}$. Note that Eq. (39) implies that the long-range molecular interaction is attractive.

The interaction force given by Eq. (39) is incorporated into the LB equation via the discrete force term. Based on our previous analysis [27], some ε^3-order terms will be caused by the discrete lattice effect on the force term, which should

be considered for multiphase flows. To cancel such effects, a consistent scheme for the ε^3-order additional term can be employed. The collision process described by Eq. (2) is then improved as

$$\begin{aligned}
\bar{\mathbf{m}} = \mathbf{m} + \delta_t \mathbf{F}_m - \mathbf{S}\left(\mathbf{m} - \mathbf{m}^{\text{eq}} + \frac{\delta_t}{2}\mathbf{F}_m\right) + \mathbf{S}\mathbf{Q}_m \\
- \mathbf{R}\left(\mathbf{I} - \frac{\mathbf{S}}{2}\right)\left(\mathbf{m} - \mathbf{m}^{\text{eq}} + \frac{\delta_t}{2}\mathbf{F}_m\right) \\
- \delta_x \mathbf{T} \cdot \nabla \rho - \frac{\delta_x}{c^2}\mathbf{X} \cdot \nabla p_{\text{LBE}},
\end{aligned} \quad (40)$$

where the discrete additional term $\mathbf{Q}_m$ is set as

$$\mathbf{Q}_m = \left[0, \ \frac{|\tilde{\mathbf{F}}|^2}{2}, \ -\frac{|\tilde{\mathbf{F}}|^2}{2}, \ 0, \ 0, \ 0, \ 0, \ \frac{\tilde{F}_x^2 - \tilde{F}_y^2}{12}, \ \frac{\tilde{F}_x \tilde{F}_y}{12}\right]^{\text{T}}, \quad (41)$$

and $\tilde{\mathbf{F}} = \mathbf{F}/(G\rho c)$. In the CE analysis, $\mathbf{F}$ is of order ε^1, and thus $\mathbf{Q}_m$ is of order ε^2 (i.e., $\mathbf{Q}_m = \varepsilon^2 \mathbf{Q}_m^{(2)}$). Considering $Q_{m,0} = Q_{m,3} = Q_{m,5} = 0$, the term $\mathbf{S}\mathbf{Q}_m$ introduced here for multiphase flows makes no difference to the previous second-order CE analysis.

A. Third-order analysis

Since the ε^3-order terms should be seriously considered for multiphase flows [27], the third-order CE analysis of the present LB model with the collision process given by Eq. (40) is carried out in this part. Note that the target of the present third-order analysis is to identify the leading-order terms at the ε^3 order. These leading-order terms are mainly related to the density gradient in the interfacial region caused by the pairwise interaction force, which means that such terms are irrelevant to time and velocity. Therefore, a steady and stationary situation can be considered, which is simple but effective and can also avoid leading to the Burnett level equation that is unnecessary and undesirable. Similarly to the second-order analysis, the ε^0-, ε^1-, ε^2-, and ε^3-order equations can be obtained from Eq. (8) by using the classical CE expansions and adding the term $\mathbf{S}\mathbf{Q}_m/\delta_t$ to the RHS of Eq. (8). In a steady and stationary situation, these ε^0-, ε^1-, ε^2-, and ε^3-order equations can be simplified as

$$\varepsilon^0 : \mathbf{m}^{(0)} = \mathbf{m}^{\text{eq}}, \quad (42a)$$

$$\varepsilon^1 : \partial_{t1}\mathbf{m}^{(0)} + \mathbf{D}_1\mathbf{m}^{(0)} - \mathbf{F}_m^{(1)} = -\frac{\mathbf{S}}{\delta_t}\left(\mathbf{m}^{(1)} + \frac{\delta_t}{2}\mathbf{F}_m^{(1)}\right), \quad (42b)$$

$$\varepsilon^2 : \partial_{t2}\mathbf{m}^{(0)} - \delta_t\mathbf{D}_1\left(\mathbf{S}^{-1} - \frac{\mathbf{I}}{2}\right)\left(\mathbf{D}_1\mathbf{m}^{(0)} - \mathbf{F}_m^{(1)}\right) = -\frac{\mathbf{S}}{\delta_t}\mathbf{m}^{(2)} + \frac{\mathbf{S}}{\delta_t}\mathbf{Q}_m^{(2)}, \quad (42c)$$

$$\varepsilon^3 : \partial_{t3}\mathbf{m}^{(0)} + \delta_t^2\left[\mathbf{D}_1\left(\mathbf{S}^{-1} - \frac{\mathbf{I}}{2}\right)\mathbf{D}_1\left(\mathbf{S}^{-1} - \frac{\mathbf{I}}{2}\right)\left(\mathbf{D}_1\mathbf{m}^{(0)} - \mathbf{F}_m^{(1)}\right) - \frac{1}{12}\mathbf{D}_1^3\mathbf{m}^{(0)}\right] + \mathbf{D}_1\mathbf{Q}_m^{(2)} = -\frac{\mathbf{S}}{\delta_t}\mathbf{m}^{(3)}, \quad (42d)$$

where the terms $\partial_{t1}\mathbf{m}^{(0)}$, $\partial_{t2}\mathbf{m}^{(0)}$, and $\partial_{t3}\mathbf{m}^{(0)}$ are reserved as a gauge for the equations at different orders.

Similarly to the second-order analysis, the equations for the conserved moments m_0, m_3, and m_5 are extracted from Eq. (42) to deduce the macroscopic conservation equation. The equations for m_0, m_3, and m_5 in the ε^1-order equation [i.e., Eq. (42b)] can be simplified as

$$\varepsilon^1 : \begin{cases} \partial_{t1}\rho = 0, \\ \partial_{t1}(\rho u_x) = -\partial_{x1}p_{\text{LBE}} + F_x^{(1)}, \\ \partial_{t1}(\rho u_y) = -\partial_{y1}p_{\text{LBE}} + F_y^{(1)}, \end{cases} \quad (43)$$

where p_{LBE} is also given by Eq. (14). Similarly, the equations for m_0, m_3, and m_5 in the ε^2-order equation [i.e., Eq. (42c)] can be simplified as

$$\varepsilon^2 : \begin{cases} \partial_{t2}\rho = 0, \\ \partial_{t2}(\rho u_x) = 0, \\ \partial_{t2}(\rho u_y) = 0. \end{cases} \quad (44)$$

After some lengthy algebra, the equations for m_0, m_3, and m_5 in the ε^3-order equation [i.e., Eq. (42d)] can be finally simplified as

$$\varepsilon^3 : \begin{cases} \partial_{t3}\rho = 0, \\ \partial_{t3}(\rho u_x) = \frac{1}{12}\delta_x^2 \nabla_1 \cdot \nabla_1 F_x^{(1)} - \frac{1}{24}c^2[2\nabla_1 \cdot (\tilde{\mathbf{F}}^{(1)}\tilde{F}_x^{(1)}) + \partial_{x1}(\tilde{\mathbf{F}}^{(1)} \cdot \tilde{\mathbf{F}}^{(1)})] \\ \qquad\qquad - \frac{1}{6}\delta_x^2[(k+1)\tau_e\tau_q - \tau_p\tau_q]\nabla_1 \cdot \nabla_1\partial_{x1}\bar{p} - \frac{1}{12}\delta_x^2(12\tau_p\tau_q - 1)\partial_{y1}^2\partial_{x1}\bar{p}, \\ \partial_{t3}(\rho u_y) = \frac{1}{12}\delta_x^2 \nabla_1 \cdot \nabla_1 F_y^{(1)} - \frac{1}{24}c^2[2\nabla_1 \cdot (\tilde{\mathbf{F}}^{(1)}\tilde{F}_y^{(1)}) + \partial_{y1}(\tilde{\mathbf{F}}^{(1)} \cdot \tilde{\mathbf{F}}^{(1)})] \\ \qquad\qquad - \frac{1}{6}\delta_x^2[(k+1)\tau_e\tau_q - \tau_p\tau_q]\nabla_1 \cdot \nabla_1\partial_{y1}\bar{p} - \frac{1}{12}\delta_x^2(12\tau_p\tau_q - 1)\partial_{x1}^2\partial_{y1}\bar{p}, \end{cases} \quad (45)$$

where $\tau_{e,p,q} = s_{e,p,q}^{-1} - 1/2$ and $\bar{p} = (3 + \beta_2)c_s^2\eta$. Combining the ε^1-, ε^2-, and ε^3-order equations [i.e., Eqs. (43)–(45)], the macroscopic equation in steady and stationary situation at the ε^3-order can be recovered as follows:

$$\begin{cases} \partial_t\rho = 0, \\ \partial_t(\rho\mathbf{u}) = -\nabla p_{\text{LBE}} + \mathbf{F} + \mathbf{R}_{\text{iso}} + \mathbf{R}_{\text{add}} + \bar{\mathbf{R}}_{\text{iso}} + \bar{\mathbf{R}}_{\text{aniso}}, \end{cases} \quad (46)$$

where $\mathbf{R}_{\text{iso}} = \frac{1}{12}\delta_x^2\nabla \cdot \nabla\mathbf{F}$ is the isotropic term caused by the discrete lattice effect, $\mathbf{R}_{\text{add}} = -\frac{1}{24}c^2\nabla \cdot [2\tilde{\mathbf{F}}\tilde{\mathbf{F}} + (\tilde{\mathbf{F}} \cdot \tilde{\mathbf{F}})\mathbf{I}]$ is the additional term introduced by $\mathbf{SQ}_m$ to cancel the effect of $\mathbf{R}_{\text{iso}}$, $\bar{\mathbf{R}}_{\text{iso}} = -\frac{1}{6}\delta_x^2[(k+1)\tau_e\tau_q - \tau_p\tau_q]\nabla \cdot \nabla\nabla\bar{p}$ and $\bar{\mathbf{R}}_{\text{aniso}} = -\frac{1}{12}\delta_x^2(12\tau_p\tau_q - 1)[\partial_y^2\partial_x\bar{p}, \partial_x^2\partial_y\bar{p}]^{\text{T}}$ are the isotropic and anisotropic terms caused by achieving self-tuning EOS, respectively. Note that $\mathbf{R}_{\text{iso}}$, $\mathbf{R}_{\text{add}}$, $\bar{\mathbf{R}}_{\text{iso}}$, and $\bar{\mathbf{R}}_{\text{aniso}}$ are all recovered at the ε^3 order and thus disappear from the macroscopic equation at the Navier-Stokes level.

B. Thermodynamic consistency

For multiphase flows, $\bar{\mathbf{R}}_{\text{iso}}$ and $\bar{\mathbf{R}}_{\text{aniso}}$ should be eliminated by setting

$$\tau_p\tau_q = (k+1)\tau_e\tau_q = 1/12, \quad (47)$$

and $\mathbf{R}_{\text{iso}}$ and $\mathbf{R}_{\text{add}}$ can be absorbed into the pressure tensor. Therefore, the pressure tensor recovered by the present LB model for multiphase flows is defined as

$$\nabla \cdot \mathbf{P} = \nabla p_{\text{LBE}} - \mathbf{F} - \mathbf{R}_{\text{iso}} - \mathbf{R}_{\text{add}}. \quad (48)$$

Performing Taylor series expansion of $\rho(\mathbf{x} + \mathbf{e}_i\delta_t)$ centered at $\mathbf{x}$, the interaction force $\mathbf{F}$ given by Eq. (39) can be expressed as

$$\mathbf{F} = G^2\delta_x^2\rho\nabla\rho + \frac{G^2\delta_x^4}{6}\rho\nabla\nabla \cdot \nabla\rho + O(\partial_{x,y}^5). \quad (49)$$

Therefore, $\mathbf{F} + \mathbf{R}_{\text{iso}} + \mathbf{R}_{\text{add}}$ in Eq. (48) can be simplified as

$$\mathbf{F} + \mathbf{R}_{\text{iso}} + \mathbf{R}_{\text{add}} = G^2\delta_x^2\rho\nabla\rho + \frac{G^2\delta_x^4}{4}\rho\nabla\nabla \cdot \nabla\rho + O(\partial_{x,y}^5). \quad (50)$$

Based on Eq. (50), the pressure tensor defined by Eq. (48) can be finally derived as follows:

$$\mathbf{P} = \left(p_{\text{EOS}} - \kappa\rho\nabla \cdot \nabla\rho - \frac{\kappa}{2}\nabla\rho \cdot \nabla\rho\right)\mathbf{I} + \kappa\nabla\rho\nabla\rho, \quad (51)$$

where $\kappa = G^2\delta_x^4/4$ and the EOS for multiphase flows is

$$p_{\text{EOS}} = p_{\text{LBE}} - \frac{G^2\delta_x^2}{2}\rho^2, \quad (52)$$

in which the self-tuning term p_{LBE} is interpreted as the incorporation of short-range molecular interaction and the second term $-G^2\delta_x^2\rho^2/2$ is due to the consideration of long-range molecular interaction. Obviously, $\mathbf{P}$ given by Eq. (51) is naturally consistent with thermodynamic theory [28], where the free energy Ψ is defined as

$$\Psi = \int_V \left(\psi_b + \frac{\kappa}{2}|\nabla\rho|^2\right)d\mathbf{x}. \quad (53)$$

Here, ψ_b is the bulk free-energy density related to EOS $p_{\text{EOS}} = \rho\partial_\rho\psi_b - \psi_b$, and $\frac{\kappa}{2}|\nabla\rho|^2$ is the interfacial free-energy density. Based on Eq. (51), the Maxwell construction can be derived.

In this work, the Carnahan-Starling EOS [29] is taken as an example:

$$p_{\text{EOS}} = K_{\text{EOS}}\left[\rho RT\frac{1 + \vartheta + \vartheta^2 - \vartheta^3}{(1 - \vartheta)^3} - a\rho^2\right], \quad (54)$$

where R is the gas constant, T is the temperature, $\vartheta = b\rho/4$, $a = 0.496388R^2T_c^2/p_c$, and $b = 0.187295RT_c/p_c$, with T_c and p_c denoting the critical temperature and pressure, respectively. The scaling factor K_{EOS} [30] is introduced here to

adjust the magnitude of bulk free-energy density ψ_b. In the Carnahan-Starling EOS, the first and second terms describe the effects of short-range (repulsive) and long-range (attractive) molecular interactions, respectively [29]. Therefore, in addition to the aforementioned thermodynamic consistency about the pressure tensor, a thermodynamic consistency between the recovered EOS [i.e., Eq. (52)] and the prescribed EOS [i.e., Eq. (54)] can also be established for the present LB model, and accordingly, the interaction strength is set as

$$G = K_{\text{INT}}\sqrt{2K_{\text{EOS}}a/\delta_x^2}, \quad (55)$$

where the scaling factor K_{INT} is introduced to adjust the interfacial free-energy density $\frac{\kappa}{2}|\nabla\rho|^2$, and the lattice sound speed is chosen as

$$c_s = K_{\text{INT}}\sqrt{\partial_\rho(p_{\text{EOS}} + K_{\text{EOS}}a\rho^2)}\Big|_{\rho=\rho_l}, \quad (56)$$

which can also achieve better numerical stability with respect to the reduced temperature T_r ($T_r = T/T_c$). With this configuration, it is known from thermodynamic theory that the surface tension σ and interface thickness W satisfy

$$\sigma \propto K_{\text{EOS}}K_{\text{INT}}, \quad W \propto K_{\text{INT}}, \quad (57)$$

where the proportionality constants can be analytically determined by the pressure tensor. Thus, in real applications of the present LB model, the surface tension and interface thickness can be independently prescribed.

IV. NUMERICAL VALIDATIONS

In this section, numerical tests, including static and dynamic cases, are carried out to validate the present LB model with self-tuning EOS for multiphase flows. The basic simulation parameters are chosen as $\varpi = 1/6$, $a = 1$, $b = 4$, $R = 1$, and $\delta_x = 1$, and a detailed implementation of the collision process [i.e., Eq. (40)] is given in Appendix B.

A. Static cases

First, a one-dimensional flat interface is simulated on a $1024\delta_x \times 4\delta_x$ domain to validate the relation $W \propto K_{\text{INT}}$. Hereafter, the interface thickness W is defined from $\rho = 0.95\rho_g + 0.05\rho_l$ to $\rho = 0.05\rho_g + 0.95\rho_l$, with ρ_g and ρ_l denoting the gas and liquid densities, respectively. Note that the present definition of W is different from the previous definition where W is obtained by fitting the density profile across interface with $\rho = 0.5(\rho_l + \rho_g) + 0.5(\rho_l - \rho_g)\tanh(2x/W)$ [19,31,32]. According to the phase-field method for multiphase flows [3,33], the present definition of W is more reasonable and the value of W is hence larger. Figure 1 shows the variation of W with K_{INT} when the reduced temperature T_r is chosen as 0.9, 0.8, 0.7, 0.6, and 0.5, respectively, and the scaling factor K_{EOS} is fixed at 1. Good proportionality between W and K_{INT} can be clearly seen. Note that when T_r is relatively small, K_{INT} should be increased to widen the interfacial region for numerical stability. Figure 2 shows the density profiles across interface for $K_{\text{EOS}} = 10^{-2}$, 10^{-1}, 10^0, 10^1, and 10^2, respectively, when $T_r = 0.8$ and $K_{\text{INT}} = 2.2949$ (i.e., $W = 10$). As one can see, the density profiles for different K_{EOS} are identical, which indicates that both the coexistence densities
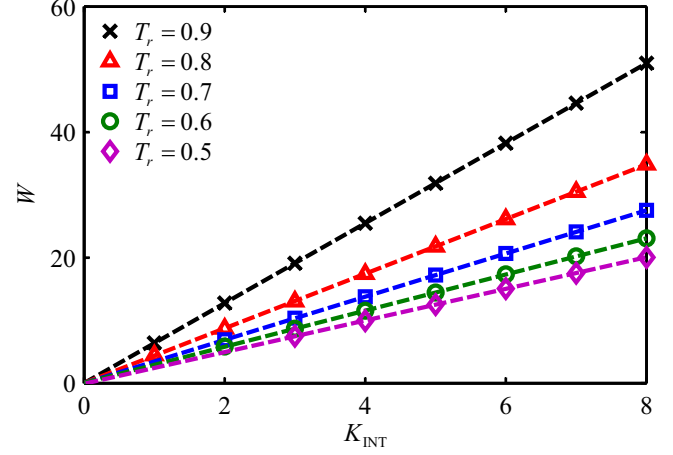

FIG. 1. Variation of the interface thickness W with the scaling factor K_{INT}. The scaling factor K_{EOS} is fixed at 1, and the dashed lines are the corresponding linear fits to the symbols.

and the interface thickness are not affected by K_{EOS}. From Fig. 2, it can also be seen that the density profile obtained by the simulation is in excellent agreement with the analytical one predicted by the pressure tensor, which validates the present LB model for multiphase flows. The coexistence curve, as a function of T_r, is then computed by slowly varying T_r, as shown in Fig. 3. Here, K_{EOS} is fixed at 1 and K_{INT} is computed by prescribing $W = 20$. It can be seen from Fig. 3 that the numerical result agrees well with the thermodynamic result by Maxwell construction. When $T_r < 0.6$, there exists a slight deviation in the gas branch, which is caused by the spatial discretization error in the interfacial region and can be reduced by increasing the interface thickness.

To validate the relation $\sigma \propto K_{\text{EOS}}K_{\text{INT}}$, a two-dimensional circular droplet is simulated on a $1024\delta_x \times 1024\delta_x$ domain with the initial diameter being $512\delta_x$. Accordingly, the surface tension is calculated via Laplace's law, i.e., $\sigma = (p_{\text{in}} - p_{\text{out}})D/2$, with p_{in} and p_{out} denoting the pressure inside and outside the droplet, respectively, and D being the final
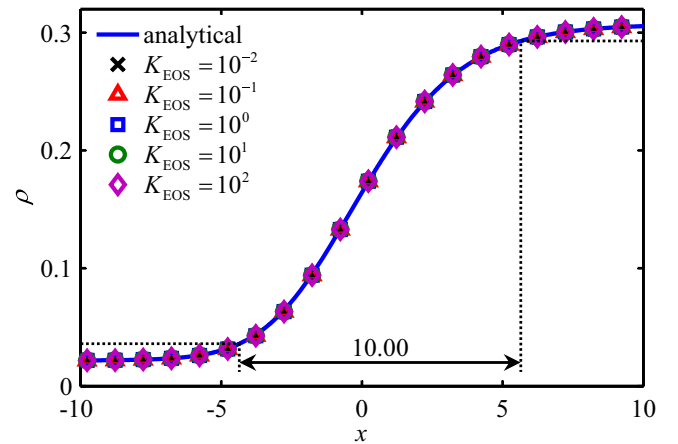

FIG. 2. Density profiles across interface obtained with various K_{EOS}. The reduced temperature T_r and the scaling factor K_{INT} are chosen as 0.8 and 2.2949, respectively.
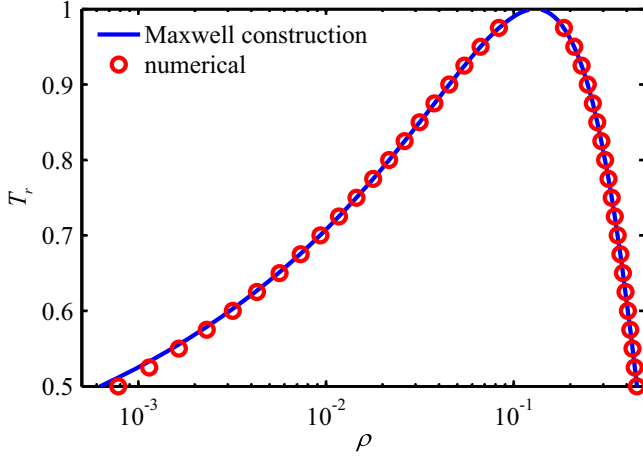
FIG. 3. Coexistence curves obtained by the simulation of a flat interface and predicted by the Maxwell construction. The scaling factor K_{EOS} is fixed at 1, and the scaling factor K_{INT} is computed by prescribing $W = 20$.

FIG. 5. Variation of the surface tension σ with the scaling factor K_{EOS}. The scaling factor K_{INT} is computed by prescribing $W = 20$ for $T_r \geqslant 0.6$ and $W = 30$ for $T_r = 0.5$, and the dashed lines are the corresponding linear fits to the symbols.

diameter of the droplet measured at $\rho = (\rho_g + \rho_l)/2$. Figure 4 shows the variation of σ with K_{INT} when $T_r = 0.9, 0.8, 0.7, 0.6,$ and 0.5, respectively, and $K_{\text{EOS}} = 1$. As one can see, σ is indeed proportional to K_{INT}. Here, it is noteworthy that, as compared with the simulation of flat interface, K_{INT} required for numerical stability significantly increases when $T_r = 0.5$. Figure 5 shows the variation of σ with K_{EOS} for various T_r when K_{INT} is computed by prescribing $W = 20$ for $T_r \geqslant 0.6$ and $W = 30$ for $T_r = 0.5$. The results in Fig. 5 demonstrate the perfect proportionality between σ and K_{EOS} and also suggest that σ can be adjusted in a wide range via K_{EOS}. Due to the excellent proportionalities observed in Figs. 1, 2, 4, and 5, the proportionality constants in Eq. (57) can then be measured by simulating a circular droplet with various K_{EOS} and K_{INT}, and the results are shown in Fig. 6. In addition, considering σ and W are physical properties that should be
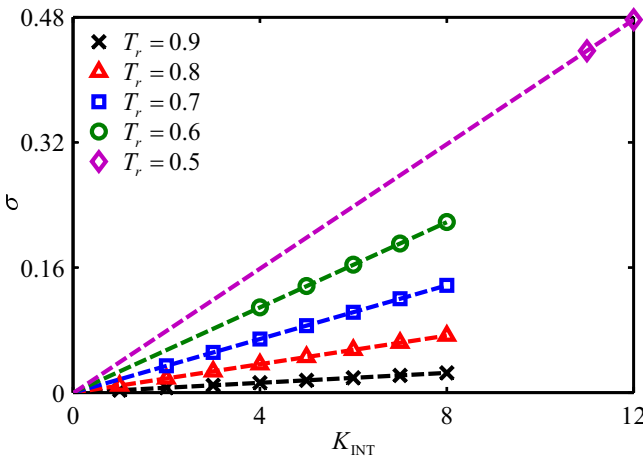
independent of the geometric configuration of the interface, σ and W predicted by the pressure tensor **P** with $K_{\text{EOS}} = K_{\text{INT}} = 1$ for a flat interface are also plotted in Fig. 6. As one can see, the numerically measured proportionality constants in Eq. (57) are in very good agreement with σ and W analytically predicted by **P**.

B. Dynamic cases

To further validate the present LB model for multiphase flows, dynamic cases are simulated in this part. First, oscillation of an elliptic droplet is simulated on a $512\delta_x \times 512\delta_x$ domain with $T_r = 0.6$, $\sigma = 0.01$, and $W = 10$, which indicates that the scaling factors are $K_{\text{EOS}} = 0.1063$ and $K_{\text{INT}} = 3.4632$. To avoid the effect of initialization, the initial semimajor and semiminor axes are set to $96.0\delta_x$ and $42.7\delta_x$, respectively, and the oscillation period T_{osi} is measured after a long time, when the oscillation becomes weak enough. The numerical results

FIG. 4. Variation of the surface tension σ with the scaling factor K_{INT}. The scaling factor K_{EOS} is fixed at 1, and the dashed lines are the corresponding linear fits to the symbols.
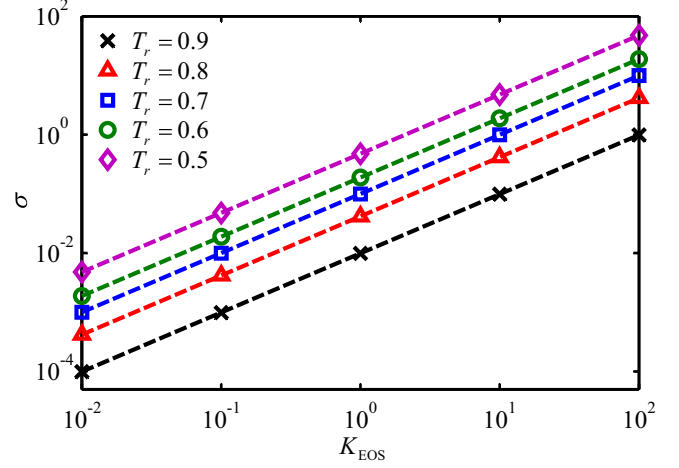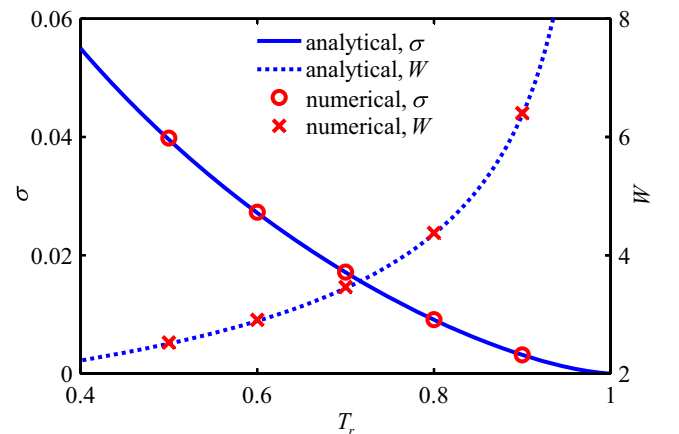

FIG. 6. Proportionality constants in Eq. (57) obtained by the simulation of a circular droplet with various K_{EOS} and K_{INT} and predicted by the pressure tensor with $K_{\text{EOS}} = K_{\text{INT}} = 1$ for a flat interface.

TABLE I. Surface tension σ, interface thickness W, and oscillation period $T_{\mathrm{osi}}/\delta_t$ obtained by the simulation of an elliptic droplet.

	σ	W	$T_{\mathrm{osi}}/\delta_t$
Numerical	0.0101105	9.96448	18346
Analytical	0.01	10	18628.0
Relative error	1.105%	−0.355%	−1.514%

are listed in Table I, where the numerical results of σ and W are measured when the oscillation finally stops and the analytical solution of T_{osi} is calculated via $2\pi[6\sigma/(\rho_l R_0^3)]^{-1/2}$ [34], in which the liquid density ρ_l and the equilibrium radius R_0 are numerically measured when the oscillation stops. As it can be seen from Table I, the present numerical results are in good agreement with the analytical solutions, which validate the present LB model and reaffirm that σ and W can be prescribed in real applications.

As a further application, head-on collision of equal-sized droplets is simulated with $T_r = 0.7$, $\sigma = 0.01$, and $W = 10$, which indicates that the scaling factors are $K_{\mathrm{EOS}} = 0.2013$ and $K_{\mathrm{INT}} = 2.9050$. The computational domain is set as $1024\delta_x \times 1024\delta_x$, and the initial droplet diameter is $128\delta_x$. The head-on collision outcome is mainly controlled by the Weber number $\mathrm{We} = \rho_l U^2 D/\sigma$ and the Reynolds number $\mathrm{Re} = UD/\nu$, with U and D denoting the relative velocity and droplet diameter, respectively. All four regimes for head-on collision, experimentally observed by Qian and Law in the three-dimensional situation [35], are successfully reproduced here in the two-dimensional situation, as shown in Fig. 7. For $\mathrm{We} = 0.01$ and $\mathrm{Re} = 1$, the droplets approach each other and then merge with small deformation. As We increases to 0.1, the droplets bounce back without merging. Here, it is worth pointing out that this "bouncing" regime is quite elusive and has not been observed in previous two- and three-dimensional simulations by the pseudopotential and free-energy LB models [36–38]. For $\mathrm{We} = 1$ and $\mathrm{Re} = 2$, and $\mathrm{We} = 20$ and $\mathrm{Re} = 100$, merging happens again, probably accompanied with large deformation in this regime. For $\mathrm{We} = 60$ and $\mathrm{Re} = 200$, the outward motion caused by strong impact splits the merged mass into three parts, with two main droplets separating from both sides and a satellite droplet residing at the center, as shown in Fig. 7(e).

V. CONCLUSION

In summary, we have developed an LB model for multiphase flows, which complies with the thermodynamic foundations of kinetic theory and thus is naturally consistent with thermodynamic theory. The underlying short-range and long-range molecular interactions are separately incorporated by constructing an LB model with self-tuning EOS and introducing a pairwise interaction force. The present model combines the advantages of the popular pseudopotential and free-energy LB models. Most computations can be carried out locally, and the surface tension and interface thickness can be independently prescribed in real applications. Numerical simulations of static cases validate the theoretical analysis of the present model for multiphase flows. As dynamic cases,
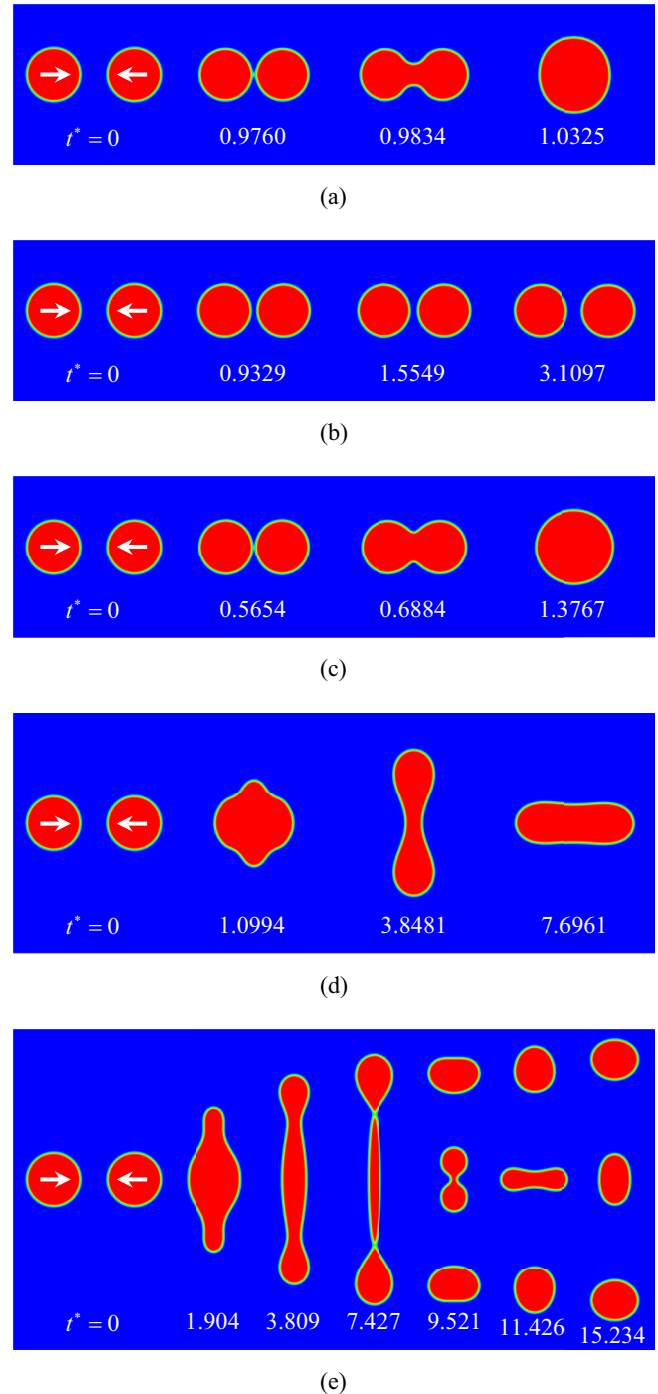

FIG. 7. Head-on collision processes of equal-sized droplets at different dimensionless time $t^* = tU/D$ with (a) $\mathrm{We} = 0.01$ and $\mathrm{Re} = 1$, (b) $\mathrm{We} = 0.1$ and $\mathrm{Re} = 1$, (c) $\mathrm{We} = 1$ and $\mathrm{Re} = 2$, (d) $\mathrm{We} = 20$ and $\mathrm{Re} = 100$, and (e) $\mathrm{We} = 60$ and $\mathrm{Re} = 200$.

oscillation of an elliptic droplet and head-on collision of equal-sized droplets are then simulated. The numerical results for oscillation are in good agreement with the analytical solutions, and all four regimes for head-on collision, including the elusive "bouncing" regime, are successfully reproduced.

It should be pointed out that the density ratio achieved by the present LB model for multiphase flows is relatively moderate. However, as an LB model with many theoretical

advantages, the present model can serve as a good framework for further developing LB models for large-density-ratio multiphase flows, which is underway and will be reported elsewhere. In addition, the present LB model with self-tuning EOS can also be applied to coupled thermo-hydrodynamic flows beyond both the Boussinesq approximation and the ideal-gas limitation, which can be found in Ref. [39].

APPENDIX A: INVERSE MATRIX

The inverse matrix of the present collision matrix **S** is

$$
\mathbf{S}^{-1} =
\begin{bmatrix}
s_0^{-1} & 0 & 0 & 0 & 0 & 0 & 0 & 0 & 0 \\
0 & s_e^{-1} & k\left(s_e^{-1}-\frac{1}{2}\right) & 0 & h\hat{u}_x\left(s_e^{-1}-\frac{1}{2}\right) & 0 & h\hat{u}_y\left(s_e^{-1}-\frac{1}{2}\right) & 0 & 0 \\
0 & 0 & s_\varepsilon^{-1} & 0 & 0 & 0 & 0 & 0 & 0 \\
0 & 0 & 0 & s_j^{-1} & 0 & 0 & 0 & 0 & 0 \\
0 & 0 & 0 & 0 & s_q^{-1} & 0 & 0 & 0 & 0 \\
0 & 0 & 0 & 0 & 0 & s_j^{-1} & 0 & 0 & 0 \\
0 & 0 & 0 & 0 & 0 & 0 & s_q^{-1} & 0 & 0 \\
0 & 0 & 0 & 0 & 2b\hat{u}_x\left(s_p^{-1}-\frac{1}{2}\right) & 0 & -2b\hat{u}_y\left(s_p^{-1}-\frac{1}{2}\right) & s_p^{-1} & 0 \\
0 & 0 & 0 & 0 & b\hat{u}_y\left(s_p^{-1}-\frac{1}{2}\right) & 0 & b\hat{u}_x\left(s_p^{-1}-\frac{1}{2}\right) & 0 & s_p^{-1}
\end{bmatrix}.
\tag{A1}
$$

APPENDIX B: IMPLEMENTATION

At first glance, the present collision process with both the cubic terms of velocity and the ε^3-order additional term considered [i.e., Eq. (40)] seems difficult to implement. However, in real applications, it can be executed in the following sequence:

$$
(1)
\begin{cases}
\bar{\mathbf{m}} \leftarrow \mathbf{m}, \\
\mathbf{m} \leftarrow \mathbf{m} - \mathbf{m}^{\mathrm{eq}}, \\
\bar{\mathbf{m}} \leftarrow \bar{\mathbf{m}} - 2\mathbf{m}, \\
\mathbf{m} \leftarrow \mathbf{m} + \frac{\delta_t}{2}\mathbf{F}_m;
\end{cases}
$$

$$
(2)
\begin{cases}
m_1 \leftarrow m_1 + \frac{1}{2}ks_\varepsilon m_2 + \frac{1}{2}hs_q(\hat{u}_x m_4 + \hat{u}_y m_6), \\
m_7 \leftarrow m_7 + bs_q(\hat{u}_x m_4 - \hat{u}_y m_6), \\
m_8 \leftarrow m_8 + \frac{1}{2}bs_q(\hat{u}_y m_4 + \hat{u}_x m_6);
\end{cases}
$$

$$
(3)\left\{\mathbf{m} \leftarrow \left[\mathbf{I} - \tfrac{1}{2}\mathrm{diag}(\mathbf{S})\right]\mathbf{m};\right.
$$

$$
(4)
\begin{cases}
\bar{m}_1 \leftarrow \bar{m}_1 - R_{11}m_1 - R_{17}m_7 - R_{18}m_8 - \delta_x \mathbf{T}_1 \cdot \nabla\rho - \frac{\delta_x}{c^2}\mathbf{X}_1 \cdot \nabla p_{\mathrm{LBE}}, \\
\bar{m}_7 \leftarrow \bar{m}_7 - R_{71}m_1 - R_{77}m_7 - R_{78}m_8 - \delta_x \mathbf{T}_7 \cdot \nabla\rho - \frac{\delta_x}{c^2}\mathbf{X}_7 \cdot \nabla p_{\mathrm{LBE}}, \\
\bar{m}_8 \leftarrow \bar{m}_8 - R_{81}m_1 - R_{87}m_7 - R_{88}m_8 - \delta_x \mathbf{T}_8 \cdot \nabla\rho - \frac{\delta_x}{c^2}\mathbf{X}_8 \cdot \nabla p_{\mathrm{LBE}};
\end{cases}
$$

$$
(5)\left\{\bar{\mathbf{m}} \leftarrow \bar{\mathbf{m}} + 2\mathbf{m};\right.
$$

$$
(6)
\begin{cases}
\bar{m}_1 \leftarrow \bar{m}_1 + s_e Q_{m,1} + k\left(\frac{1}{2}s_e - 1\right)s_\varepsilon Q_{m,2}, \\
\bar{m}_2 \leftarrow \bar{m}_2 + s_\varepsilon Q_{m,2}, \\
\bar{m}_7 \leftarrow \bar{m}_7 + s_p Q_{m,7}, \\
\bar{m}_8 \leftarrow \bar{m}_8 + s_p Q_{m,8};
\end{cases}
$$

where "$\leftarrow$" indicates assignment, and $\mathrm{diag}(\mathbf{S})$ denotes the diagonal part of the present collision matrix **S**. Here, steps (1), (3), and (5) are the same as those for the classical multiple-relaxation-time (MRT) collision process, step (2) corresponds to the improvement of the collision matrix, step (4) corresponds to the elimination of the cubic terms of velocity, and step (6) corresponds to the introduction of the ε^3-order

additional term. In step (4), $\nabla\rho$ and ∇p_{LBE} can be locally evaluated resorting to the interaction force [i.e., Eq. (39)] as follows:

$$
\nabla\rho = \frac{\mathbf{F}}{G^2\delta_x^2\rho}, \qquad \nabla p_{\mathrm{LBE}} = \left(\frac{dp_{\mathrm{EOS}}}{d\rho} + G^2\delta_x^2\rho\right)\frac{\mathbf{F}}{G^2\delta_x^2\rho}. \tag{B1}
$$

From the above discussion, it can be seen that the present collision process is actually easy to implement, and all the involved computations can be locally performed except for the simple interaction force. Therefore, compared with the pseudopotential LB model known as the simplest multiphase LB model, no additional computational complexity is introduced in the present LB model. Based on our numerical test, the computational cost of the present model is only 1.178 times as much as that of a pseudopotential MRT LB model by Li *et al.* [34].

[1] G. R. McNamara and G. Zanetti, Phys. Rev. Lett. **61**, 2332 (1988).

[2] A. K. Gunstensen, D. H. Rothman, S. Zaleski, and G. Zanetti, Phys. Rev. A **43**, 4320 (1991).

[3] Q. Li, K. H. Luo, Q. J. Kang, Y. L. He, Q. Chen, and Q. Liu, Prog. Energy Combust. Sci. **52**, 62 (2016).

[4] X. Shan and H. Chen, Phys. Rev. E **47**, 1815 (1993).

[5] M. R. Swift, W. R. Osborn, and J. M. Yeomans, Phys. Rev. Lett. **75**, 830 (1995).

[6] X. He, X. Shan, and G. D. Doolen, Phys. Rev. E **57**, R13 (1998).

[7] L.-S. Luo, Phys. Rev. Lett. **81**, 1618 (1998).

[8] X. He and G. D. Doolen, J. Stat. Phys. **107**, 309 (2002).

[9] X. Shan and H. Chen, Phys. Rev. E **49**, 2941 (1994).

[10] M. Sbragaglia, R. Benzi, L. Biferale, S. Succi, K. Sugiyama, and F. Toschi, Phys. Rev. E **75**, 026702 (2007).

[11] Q. Li, K. H. Luo, and X. J. Li, Phys. Rev. E **86**, 016709 (2012).

[12] S. Khajepor, J. Wen, and B. Chen, Phys. Rev. E **91**, 023301 (2015).

[13] M. R. Swift, E. Orlandini, W. R. Osborn, and J. M. Yeomans, Phys. Rev. E **54**, 5041 (1996).

[14] D. J. Holdych, D. Rovas, J. G. Georgiadis, and R. O. Buckius, Int. J. Mod. Phys. C **9**, 1393 (1998).

[15] T. Inamuro, N. Konishi, and F. Ogino, Comput. Phys. Commun. **129**, 32 (2000).

[16] A. N. Kalarakis, V. N. Burganos, and A. C. Payatakes, Phys. Rev. E **65**, 056702 (2002).

[17] A. N. Kalarakis, V. N. Burganos, and A. C. Payatakes, Phys. Rev. E **67**, 016702 (2003).

[18] X. He, S. Chen, and R. Zhang, J. Comput. Phys. **152**, 642 (1999).

[19] T. Lee and C.-L. Lin, J. Comput. Phys. **206**, 16 (2005).

[20] R. Huang, H. Wu, and N. A. Adams, Phys. Rev. E **97**, 053308 (2018).

[21] M. E. McCracken and J. Abraham, Phys. Rev. E **71**, 036701 (2005).

[22] P. Lallemand and L.-S. Luo, Phys. Rev. E **61**, 6546 (2000).

[23] Y. H. Qian, D. d'Humières, and P. Lallemand, Europhys. Lett. **17**, 479 (1992).

[24] P. J. Dellar, J. Comput. Phys. **259**, 270 (2014).

[25] P. J. Dellar, Phys. Rev. E **65**, 036309 (2002).

[26] S. Chapman and T. G. Cowling, *The Mathematical Theory of Non-Uniform Gases*, 3rd ed. (Cambridge University Press, Cambridge, 1970).

[27] R. Huang and H. Wu, J. Comput. Phys. **327**, 121 (2016).

[28] J. S. Rowlinson and B. Widom, *Molecular Theory of Capillarity* (Oxford University Press, Oxford, 1982).

[29] N. F. Carnahan and K. E. Starling, J. Chem. Phys. **51**, 635 (1969).

[30] A. J. Wagner and C. M. Pooley, Phys. Rev. E **76**, 045702 (2007).

[31] D. Lycett-Brown and K. H. Luo, Phys. Rev. E **94**, 053313 (2016).

[32] A. Fakhari, T. Mitchell, C. Leonardi, and D. Bolster, Phys. Rev. E **96**, 053301 (2017).

[33] V. E. Badalassi, H. D. Ceniceros, and S. Banerjee, J. Comput. Phys. **190**, 371 (2003).

[34] Q. Li, K. H. Luo, and X. J. Li, Phys. Rev. E **87**, 053301 (2013).

[35] J. Qian and C. K. Law, J. Fluid Mech. **331**, 59 (1997).

[36] D. Lycett-Brown, I. Karlin, and K. H. Luo, Commun. Comput. Phys. **9**, 1219 (2011).

[37] D. Lycett-Brown, K. H. Luo, R. Liu, and P. Lv, Phys. Fluids **26**, 023303 (2014).

[38] A. M. Moqaddam, S. S. Chikatamarla, and I. V. Karlin, Phys. Fluids **28**, 022106 (2016).

[39] R. Huang, H. Wu, and N. A. Adams, arXiv:1809.08683.